Biogeochemical spatio-temporal transformation of copper in Aspergillus niger colonies grown on malachite with different inorganic nitrogen sources

Fomina, Marina; Bowen, Andrew D.; Charnock, John M.; Podgorsky, Valentin S.; Gadd, Geoffrey M.

Published in:
Environmental Microbiology

DOI:
10.1111/1462-2920.13664

Publication date:
2017

Document Version
Peer reviewed version

Biogeochemical spatio-temporal transformation of copper in *Aspergillus niger* colonies grown on malachite with different inorganic nitrogen sources

Marina Fomina[1,2], Andrew D. Bowen[1], John M. Charnock[3], Valentin S. Podgorsky[2] and Geoffrey M. Gadd[1,4*]

[1] *Geomicrobiology Group, School of Life Sciences, University of Dundee, Dundee DD1 5EH, Scotland, UK*

[2] *Institute of Microbiology and Virology, NASU, Zabolotnogo st. 154, Kiev 03680, Ukraine*

[3] *School of Earth, Atmospheric and Environmental Sciences, University of Manchester, Williamson Building, Oxford Road, Manchester M13 9PL, UK*

[4] *Laboratory of Environmental Pollution and Bioremediation, Xinjiang Institute of Ecology and Geography, Chinese Academy of Sciences, Urumqi 830011, China*

*Correspondence:

Professor Geoffrey Michael Gadd, Geomicrobiology Group, School of Life Sciences, University of Dundee, DD1 5EH, Scotland, UK.

Tel.: +44 1382 384767; E-mail: g.m.gadd@dundee.ac.uk

Running title: Spatio-temporal copper speciation in fungal colonies

Summary

This work elucidates spatio-temporal aspects of the biogeochemical transformation of copper mobilized from malachite ($Cu_2(CO_3)(OH)_2$) and bioaccumulated within *Aspergillus niger* colonies when grown on different inorganic nitrogen sources. It was shown that the use of either ammonium or nitrate determined how copper was distributed within the colony and its microenvironment and the copper oxidation state and succession of copper coordinating ligands within the biomass. Nitrate-grown colonies yielded ~1.7× more biomass, bioaccumulated ~7× less copper, excreted ~1.9× more oxalate and produced ~1.75× less water-soluble copper in the medium in contrast to ammonium-grown colonies. Microfocus X-ray absorption spectroscopy (XAS) revealed that as the mycelium matured, bioaccumulated copper was transformed from less stable and more toxic Cu(I) into less toxic Cu(II) which was coordinated predominantly by phosphate/malate ligands. With time, a shift to oxalate coordination of bioaccumulated copper occurred in the central older region of ammonium-grown colonies.

Keywords: Copper speciation, mineral transformations, *Aspergillus niger*, fungal colony, oxalate, microfocus XAS

Introduction

Fungi in both terrestrial and aquatic ecosystems are responsible for many fundamental ecological processes including the cycling of metals and other elements, especially C, N, P and S. Elucidation of the molecular nature of toxic metal immobilization by fungi is of relevance to obtaining a fuller understanding of the chemical and biological interactions of organisms with environmental pollutants and to the development of efficient bioremediation and biorecovery techniques. However, spatio-temporal aspects of the biogeochemical transformation of toxic metals mobilized from minerals and bioaccumulated within fungal colonies remains poorly understood.

Being highly reactive, copper has the ability to interact with soil minerals and organic components resulting in variations of Cu bioavailability in different soils (Dumestre *et al*., 1999). Many fungi are able to withstand copper toxicity, and can effect biogeochemical transformations of copper through proton- and ligand-promoted metal mobilization from insoluble copper compounds with consequent metal immobilization within biomass and/or in the microenvironment (Fomina *et al*., 2004, 2005a,b; 2007a,b). Fungi provide a number of ligands for both metal mobilization and immobilization. For example, carboxylate ligands can result from low molecular weight organic acids such as oxalate, citrate and acetate which are produced by many fungal species (Dutton and Evans, 1996; Gadd, 1999). Among them, oxalate is a key metabolite that plays a significant role in many metal and mineral transformations mediated by fungi (Gadd *et al*., 2014). Oxalic acid is a relatively strong acid and the oxalate anion is able to complex metals, resulting in formation of metal-oxalate complexes and/or precipitation of insoluble metal oxalates depending on the metal and chemical conditions (Arnott, 1995; Fomina *et al*., 2005a; Gadd *et al*., 2014). The production and excretion of oxalic and other organic acids by fungi appears to be enhanced by nitrate nutrition compared to ammonium nutrition (Lapeyrie *et al*., 1987; Gadd, 1999).

Previous geomycological studies of toxic metal speciation within fungal biomass using bulk fixed-beam X-ray absorption spectroscopy (XAS) revealed that oxygen ligands such as carboxylate and phosphate play a major role in copper coordination within fungal and ectomycorrhizal biomass exposed to copper-containing minerals (Fomina *et al*., 2007a). For *Aspergillus niger* grown with malachite or azurite, the coordination of bioaccumulated copper varied in different regions of the colony showing phosphate ligands in the central zone and a copper sulfide phase in the peripheral zone (Fomina *et al*., 2007a). For the ectomycorrhizal fungus *Rhizopogon rubescens* grown in the presence of copper phosphate, it was shown that the coordination of bioaccumulated copper depended on the inorganic nitrogen source revealing oxalate coordination of copper on nitrate (Fomina *et al*., 2007a). For some samples in these studies, the coordination environment for copper was heterogeneous which indicated the presence of mixed ligands (Fomina *et al*., 2007a).

In considering that both nitrogen source and the age of the fungal mycelium may affect copper speciation and the obvious limitations of bulk XAS, it appears essential to carry out a comprehensive study of the spatio-temporal biogeochemical transformation of copper within the fungal colony and its microenvironment. Such work requires a combination of conventional geomicrobiological methods with an advanced solid state chemistry approach, microfocus XAS, which will provide better resolution of the ligands surrounding the target metal. The aim of this work was therefore to study the spatio-temporal dynamics of the biogeochemical transformation of copper by fungal colonies and its relationship to the inorganic nitrogen source present using the ubiquitous geoactive fungus *A. niger* exposed to the copper-bearing mineral malachite.

Results and discussion

Initial evaluation of growth and copper accumulation showed that radial growth of *A. niger* colonies on control malachite-free media was not significantly affected by the inorganic nitrogen source with extension rates being around 5 mm·day^{-1} (Fig. 1 A, B). If the agar medium was amended with 10 mM malachite, radial growth of the fungus on ammonium was considerably inhibited (~40%) with the extension rate generally < 3 mm.day^{-1}. The formation of a clear mineral solubilization halo around the colony in ammonium- and malachite-amended agar was observed, expanding in correlation with radial growth. A clear zone of malachite solubilization did not develop in the presence of nitrate despite the active radial growth. This could be a result of insufficient malachite solubilization or rapid transformation of mobilized copper into abundant secondary minerals. In addition, the presence of ammonium in the medium may enhance the solubility of malachite. This phenomenon has been previously described in geochemical modelling studies of abiotic chemical systems with malachite and ammonia and/or ammonium chloride (Wang et al., 2009). In our study, enhanced mineral dissolution in the presence of ammonium could also result in increased mobility of copper.

The biomass yield of fungal colonies exposed to malachite significantly differed between the tested nitrogen sources in agreement with the tendencies observed for radial growth (Fig. 1C). *A. niger* biomass grown on nitrate-containing medium for 1 week was ~1.7× higher than that produced on ammonium-containing medium ($P<0.05$). The rate of biomass increase in the nitrate-grown colony (16.3 mg.day^{-1}) was more than 1.5× higher than that for ammonium-containing medium (10.3 mg.day^{-1}) ($P<0.05$). The tolerance index (TI) for malachite was 107.5% on nitrate medium being almost 1.5 times higher than the TI on ammonium-containing medium (77.5%).

The use of different inorganic sources of nitrogen induced differences in the morphology of *A. niger* colonies exposed to malachite with ammonium causing numerous ridges to form in

the mycelium and considerably reducing the formation of conidia. In this case, the central dark conidia-forming zone was only about 30% of the colony surface area whereas on nitrate-containing medium this zone covered almost 80% of the colony (Fig. S1A, S2A,D).

Bioaccumulation of copper mobilized from malachite significantly differed ($P < 0.05$) between the two inorganic nitrogen sources (Fig. 1D). The final amount of accumulated copper was considerably higher for ammonium-containing medium (25 mg (g dry wt)$^{-1}$) than for nitrate-containing medium (3 mg.(g dry wt)$^{-1}$). This difference between ammonium- and nitrate-containing media varied during the growth period being 23 times higher on the first day and 7 times higher on the seventh day. For both nitrogen sources, the time course of copper accumulation by the biomass showed apparent saturation commencing at the fifth day which suggests biogeochemical equilibration within the microcosm at this point. The increased copper bioaccumulation observed for ammonium-containing medium coincided with both the visual manifestation of a clear zone of malachite solubilization in the agar and reduced growth in terms of radial extension and biomass yield. These data suggest more active solubilization of malachite with consequent enhanced toxic effects of mobilized copper on *A. niger* in the presence of ammonium.

Analysis of pH profiles showed that ammonium-containing medium was characterised by a more spatially heterogeneous pH decrease after 7 days with a pronounced decline in the centre of the microcosm compared to nitrate-containing medium (Fig. 1 E, F). The initial pH value (pH 5.3) for nitrate-containing medium was lower than that for ammonium (pH 5.8). During growth on nitrate, there was a rapid decline in pH in the centre of the microcosm on the 3rd day with the consequent equilibration of these values around pH 3 over the whole microcosm after 7 days.

To study the spatio-temporal transformation of copper in the agar throughout the whole microcosm, a sequential elution technique was used which provided information on copper speciation in the different fractions: H_2O, NaCl, NH_4OH, CH_3COOH and HCl (Fomina *et al*., 2005a) (Fig. 2). The water fraction represents water-soluble copper, the NaCl fraction evaluates

electrostatically adsorbed and ion-exchangeable copper in the sample, and the NH_4OH fraction shows the presence of some copper-bearing minerals including malachite. The CH_3COOH and HCl fractions were used to evaluate the amount of copper associated with other compounds such as oxides. Additional extraction of copper with concentrated HNO_3 was used to detect any copper remaining after sequential elution but this was usually insignificant. Almost all the malachite (> 90 %) was dissolved by NH_4OH. However, biomineralization of mobilized copper as copper oxalate could also be included in the NH_4OH-fraction. To distinguish copper bound within malachite from copper immobilized as copper oxalate in the NH_4OH-fraction, it was therefore essential to complement the sequential elution data with oxalic acid profiling in the agar (see later).

The use of either ammonium or nitrate as a nitrogen source led to significant differences in the dynamics and profile of copper present in the different fractions extracted from agar during growth of *A. niger* (Figs. 2, 3). For ammonium, it was observed there was a significantly higher copper decline over time in the NH_4OH-fraction representing the minerals in the colony microenvironment (Figs. 2, 3A). At the seventh day of growth, the copper concentration in the NH_4OH-fraction reached its minimal value across the microcosm ranging from approximately 0-2 mM whereas for nitrate this varied over the range 2-4 mM. At the third day of growth on ammonium medium, there were also sharper differences between the quantities of NH_4OH–eluted copper in central and peripheral parts of the microcosm, with little detected beneath the centre of the colony and ~7 mM beneath the peripheral zone. The quantity of water-soluble copper in the agar gradually increased with colony growth from the centre of the microcosm reaching 3-4 mM at day 3 becoming eventually balanced at around this concentration at day 7 (Figs. 2, 3B). By the end of the cultivation period on ammonium-containing medium, water-soluble copper comprised the majority of all copper left in the agar which was consistent with the high level of copper bioaccumulated by the biomass. Growth on nitrate-containing medium led to a more homogeneous distribution of NH_4OH–eluted mineral phase copper (Figs. 2, 3A). It

was also noted that there was a more rapid initial decrease in copper in this fraction between the first and the third day of growth which probably reflected a faster initial increase in water-soluble copper reaching 3-4 mM in the centre of the microcosm two days earlier than for ammonium-containing medium (Figs. 2, 3B). The subsequent sharp increase in water-soluble copper at day 3 reaching 4-5 mM in ~75% of the agar volume can be explained by both the sharp decline in pH at this time and an increase in oxalate excretion by the fungus. Over the 5^{th} -7^{th} days, the water-soluble copper in the agar decreased to 2-3 mM across the whole microcosm. Thus, in nitrate-containing medium, the fungal microenvironment contained less bioavailable mobile copper than in ammonium-containing medium.

To evaluate oxalic acid in the medium, water- and HCl-extraction was used. The water-fraction represents free oxalate whereas the HCl-fraction shows oxalate bound with copper as copper oxalate. After the first day, the total amount of oxalate (as the sum of water- and HCl-extractable) in the centre of the microcosm was the same for both ammonium- and nitrate-containing media reaching around 2 mM (Fig. 4). However, the amount of oxalate in the colony peripheral zone (at 35 mm from the centre of the plate) was considerably higher (>5x) in ammonium- (1.79 mM) than nitrate-containing medium (0.35 mM) ($P<0.05$). In contrast to ammonium, on nitrate-containing medium the total oxalate concentration generally increased across the microcosm during days 3-7 reaching maximum values of ~4.5 mM. In central regions of the nitrate-containing microcosm, the amount of oxalate was generally higher than in peripheral regions. For ammonium-containing medium, the HCl-fraction of oxalate reached 1mM in the centre of the microcosm on the first day being twice the value for the colony periphery. After this time the value varied across the microcosm over the approximate range of 1 – 1.5 mM. The dynamics and spatial distribution of water-extractable oxalate was generally similar to HCl-extractable copper though the values for free oxalate were rather lower.

In nitrate-containing medium, the dynamics and spatial distribution of water-extractable oxalate significantly differed from that of HCl-extractable oxalate (Fig. 4). The water-fraction

was considerably lower across the whole microcosm being < 0.2 mM at day 1 and reaching 1.5 mM at day 7. In contrast to free oxalate, at day 1 the amount of HCl-extractable oxalate reached a value of 2 mM in the centre of the microcosm beneath the growing colony significantly exceeding the value at the periphery (~0.35 mM). At the third day, at a distance of 15-25 mm from the microcosm centre, there was a sharp rise in HCl-extractable oxalate reaching approximately 3 mM. Subsequently, these values varied over the range of 2 - 3 mM across the microcosm which could be related to enhanced precipitation of copper mobilized from malachite as copper oxalate.

Analysis of the proportion of the water-fraction that was oxalate showed that for ammonium-containing medium at day 1 this fraction varied over the range of 60-80% of the total oxalate in the microcosm (Fig. 4). This was on average around 14-times lower for nitrate-containing medium reaching a maximum value of ~ 9% in the centre of the microcosm. At the third day, the centre of the microcosm showed around 40% oxalate for both nitrogen sources declining for ammonium-containing medium and abruptly rising in the presence of nitrate. By day 7, the proportion of water-extractable oxalate was balanced across the whole microcosm providing similar values around 32 - 39% for both ammonium- and nitrate- containing media. In general, the total amount of oxalate was ~1.6-1.9 times higher in nitrate- than in ammonium-containing medium. The pronounced quantitative prevalence of HCl-extractable oxalate after growth on nitrate probably indicates extensive oxalate binding of the copper mobilized from the malachite. Such enhanced copper oxalate biomineralization by *A. niger* when growing on nitrate explains the significantly lower copper bioaccumulation in the biomass.

Integration of the data on copper bioaccumulated within the colonies, amounts of copper eluted within the different fractions, and HCl-extractable oxalate allowed evaluation of the distribution of copper between the biomass and the colony microenvironment (Table 1). It is clear that the inorganic nitrogen source largely defined how copper was distributed between the medium and biomass and its chemical speciation. In nitrate-containing medium, the proportion

of copper removed from the medium and accumulated by the fungus was only ~8% whereas for ammonium-containing medium, the fungus accumulated over one third of the copper (~37%) and almost half the total microcosm copper (~49%) remained in the microenvironment in a bioavailable mobile form as represented by the extracted water-soluble fraction. The proportion of copper in the water-soluble fraction for the nitrate-containing medium was ~28% being 1.75 times lower than that for ammonium. A significant 5-fold rise in the proportion of ion-exchangeable copper in the NaCl-fraction was observed for nitrate-containing medium when compared to ammonium -containing medium.

Dissolution of malachite was ~66-times higher in ammonium-containing medium (Table 1). In general, the NH_4OH-fraction, which represented primary and/or secondary mineral phases, comprised ~8% for ammonium-containing medium being approximately 4.5 times lower than with nitrate (~36%). Consequently, a clear solubilization zone was not observed in nitrate-containing medium. Using data on the concentration of HCl-extractable oxalate, the copper located within minerals could be divided into two fractions: (1) copper within the malachite and (2) copper within copper oxalate. For ammonium-containing medium, the malachite fraction of copper was negligible and ~8% of copper in the mineral phase was bound as oxalate. For nitrate-containing medium, the proportion of copper within copper oxalate was 16.5% whereas 20% of the copper was located within the malachite. Such comparative impacts of proton- and ligand-promoted mechanisms of malachite transformation was further evaluated by regression analysis. The most significant factor for copper bioaccumulation on ammonium-containing medium was found to be acidification ($P < 0.001$) in contrast to oxalate excretion ($P<0.01$). The opposite was observed for nitrate-containing medium where oxalate excretion was of high significance ($P<0.001$) for copper bioaccumulation being complemented by the lower significance of acidification ($P<0.01$).

Further detailed study of the spatio-temporal speciation of copper bioaccumulated by *A. niger* colonies was carried out using microfocus XAS with a beam size of a few micrometres.

The X-ray beam was focused on specific points in the colony corresponding to mature conidia-forming mycelium in the centre and juvenile marginal mycelium in the colony periphery after growth for 5 and 10 days. The results of microfocus XAS demonstrated considerable differences between colonies grown on ammonium and nitrate (Figs 5, S1, S2). In agreement with the AAS data, the microfocus XAS maps also showed significantly higher amounts of bioaccumulated copper on ammonium-containing medium (Figs. 1D, 5, S1, S2). *A. niger* colonies grown on ammonium showed enhanced copper accumulation in the centre of the colony and substantial metal concentrations located within thick mycelial ridges in contrast to nitrate (Figs. 5, S1). For all the XANES spectra, oxygen atoms gave the best fit for the inner coordination shell surrounding the copper. Identification of elements in the outer coordination shells was complicated by spectral noise reflecting the rather low copper concentration at the tested points and probably mixed coordination of copper by different oxygen-containing ligands such as phosphate and carboxylate. Another common feature found in XANES spectra of biomass grown on ammonium-containing medium was a decrease in the shoulder at approximately 8980 eV when approaching the centre of the colony which reflected the tendency of a decreased proportion of Cu(I) in bioaccumulated copper with mycelium maturation (Fig. 5D). Microfocus XAS performed on conidia from the centre of the five-day colony grown on ammonium revealed that bioaccumulated copper was present exclusively as Cu(II) and most likely coordinated by phosphate and/or malate ligands. After 10 day growth on ammonium-containing medium, a green colouration of the mycelium related to higher copper bioaccumulation developed and the proportion of the conidia-forming zone decreased (Fig. S1A). Elemental mapping showed a high copper concentration in the colony centre and in the mycelial ridges (Fig. S1B). A significant difference in copper oxidation state and coordination was revealed between the mature mycelium in the colony centre which contained Cu(II) coordinated by oxalate and younger conidia-free mycelium at the periphery which contained Cu(I) (Fig. S1C).

Both 5- and 10-day nitrate-grown colonies significantly differed from ammonium-grown colonies by an extensive conidia-forming zone and homogeneous copper distribution across the colony with a low concentration of bioaccumulated copper leading to the weak signals in the collected spectra (Fig. S2). Nevertheless, comparison of the absorption edge for mature and juvenile mycelium demonstrated the same tendency as for the ammonium-grown 5 day colony with a shift at 8980 eV (Fig. S2A-C). This suggested that for the 5 day *A. niger* colony grown on nitrate, the majority of bioaccumulated copper in the periphery was present as Cu(I) whereas mature mycelium in the centre of the colony showed the dominance of Cu(II) coordinated by either malate or phosphate. However, for the 10 day nitrate-grown colony, the oxidation state of bioaccumulated copper and the nature of its coordination environment did not differ between mature and marginal mycelium (Fig. S2F) and XANES data indicated that Cu(II) was most likely coordinated by phosphate and/or malate.

It can be concluded therefore that the source of inorganic nitrogen substantially affected spatio-temporal changes in oxidation state and the coordination environment of the copper bioaccumulated by *A. niger* exposed to malachite. On ammonium-containing medium dominance of Cu(I) was retained in younger peripheral regions while Cu(II) speciation shifted from malate/phosphate to oxalate coordination in the older central zone of the colony (Fig. 6). For nitrate-containing medium, malate/phosphate coordination of copper (II) was retained in the colony centre in contrast to the peripheral region where the initial prevalence of Cu(I) shifted to malate/phosphate copper (II) coordination and eventual homogeneous copper speciation across the whole colony. This indicates that as the fungal mycelium is maturing, bioaccumulated copper is transformed from the less stable and more toxic Cu(I) into less toxic Cu(II). Mobile Cu(I) is harmful to living cells as it can cross cell membranes and form free radicals, such as the hydroxyl free radical, reacting with any oxidizable substrate and damaging important biomolecules (Outten *et al*., 2001; Rensing and Grass, 2003; Bellion *et al*., 2006). The fungus would benefit from an ability to sequester Cu(I) by copper-binding cysteine-rich

metallothioneins. Due to the low local copper concentration in the peripheral region of the colony, it was difficult to identify the coordination environment for Cu(I) using microfocus XAS. However, it is likely that Cu(I) was coordinated with sulfur ligands (Fomina *et al*., 2007a). Metallothioneins play an important role in Cu homeostasis and sequestration (Jaeckel *et al*., 2005; Kumar *et al*., 2005). It is likely that the majority of copper sequestration in juvenile mycelia occurs by this mechanism and other studies have identified a metallothionein in *A. niger* (Kermasha *et al*., 1993; Goetghebeur *et al*., 1995). The structure of a fungal copper metallothionein has been described showing four Cu atoms chelated by eight cysteines to produce a copper (I) sulfur centre (Bordas *et al*., 1983). The reductive transformation of Cu(II) from the malachite to Cu(I) while being bioaccumulated by juvenile mycelium in the peripheral zone can be explained by a decrease in redox potential during growth on the nutrient-rich medium. Eventually the depletion of nutrients by the growing and aging fungus is associated with an increase in redox potential leading to the prevalence of Cu(II) within the bioaccumulated copper.

In our study, as the proportion of Cu(II) increased with aging of the mycelium regardless of the nitrogen source used, microfocus XAS revealed a shift in copper speciation to phosphate and/or carboxylate (malate or oxalate) coordination (Fig. 6). In general, mixed phosphate/malate ligands prevailed for Cu(II) coordination in malachite-grown *A. niger*. The phosphate groups in fungal biomass can be of organic and inorganic origin (e.g. nucleic acids, adenosine phosphates, polyphosphates) and precipitation of secondary metal phosphates originating from initial metal phosphates can also occur. Polyphosphates are linear polymer chains of orthophosphate residues linked by phosphoanyhydride bonds serving a wide range of functions including metal-phosphate precipitation which effectively sequester the toxic metal species preventing them from causing cellular damage (Orlovich and Ashford, 1993; Bücking and Heyser, 1999; Kornberg *et al*., 1999, de Souza *et al.*, 2005; Saito *et al*., 2005; 2006). Vacuolar polyphosphates can immobilize metals in ectomycorrhizal fungi (Bucking and Heyser, 1999). The specific pathways

that control polyphosphate production, and the mechanisms by which they immobilize metals vary between species and are controlled by a wide range of enzymes affected by environmental conditions and the fungal growth-phase (Tsekova *et al*., 2002; Tsekova and Galabova, 2003). Such variations may explain the shift to phosphate coordination of copper with maturation of the *A. niger* mycelium. Carboxyl groups are also involved in immobilization of bioaccumulated copper together with phosphates. These can be derived from, e.g. low molecular weight organic acids (LMWOA), proteins, polysaccharides, (poly)phenols/quinones, and melanin (Fomina *et al*., 2007a). LMWOA such as malate, oxalate, citrate and acetate can form strong complexes with metal cations (Jones, 1998; van Hees *et al.*, 2001). Many fungal species can produce LMWOA, both free-living and symbiotic fungi (Dutton and Evans, 1996; Gadd, 1999; Gadd *et al*., 2014). In some LMWOA producing fungi, the production of certain organic acids appears to be enhanced by nitrate nutrition (Lapeyrie *et al.*, 1987; Gadd, 1999).

Nitrate uptake and reductive assimilation to ammonia via nitrate reductase leads to proton consumption resulting in an intracellular imbalance of electrical charge and perturbations in cytosolic pH. Intracellular pH stabilization is mainly ensured by two mechanisms: (i) the excretion of OH- from the cells into the external medium, and (ii) the synthesis of carboxylate and protons (Davies, 1986). Most of the oxalate produced by fungi is excreted from the cell preventing irreversibility of oxalate synthesis in response to a decrease in cytosolic pH. Oxalate is transported in ionic form because the cytosolic pH (around pH 7) is higher than the pK of oxalic acid (pK for $oxalate^{-}/oxalate^{2-}$ is 4.19), meaning that the organic acid is present as an anion in the cytosol. When carboxylates are excreted as anions, their charge can be balanced by cation efflux such as $C_2O_4^{2-}/2H^+$ (Roelofs *et al.*, 2001). If ammonium is used as a sole source of nitrogen, exchange of NH_4^+ and H^+ between the cell and the environment provides electronic neutrality. Consumed NH_4^+ serves as the main sink for carbon skeletons for amino acid synthesis competing with LMWOA synthesis (Carrodus, 1967) as well inhibiting glyoxylate

dehydrogenase activity (Kritzman *et al.*, 1977). Both phenomena may lead to reduced production and excretion of LMWOA including oxalate.

In this work, the change of inorganic nitrogen source from ammonium to nitrate significantly promoted oxalate excretion resulting in extensive precipitation of copper oxalate. It is well known that fungal oxalate readily forms complexes with toxic metals consequently forming stable mycogenic minerals including copper oxalate hydrate (moolooite) (Fomina *et al*., 2005a; Gadd, 2007; Gadd *et al*, 2014). In contrast to nitrate-grown mycelium which clearly released synthesized oxalate out of the cells, *A. niger* grown on ammonium-containing medium with malachite showed apparent oxalate coordination of copper within the mature central mycelium (Fig. 6). There is no strong evidence that mycogenic oxalates may occur intracellularly. However, electron microscopic (ESEM) examination of the mycelium did not reveal any obvious extracellular biomineralization. This suggests that the bioaccumulated copper may be amorphously bound to oxalate ligands within the hydrated extracellular sheath. It cannot be ruled out that some oxalate coordination of copper might represent an intracellular vacuolar oxalate, possibly as a result of reduced oxalate efflux during growth on ammonium.

In conclusion, we have shown that the relative roles of proton- and ligand- promoted dissolution of malachite by *A. niger* was considerably influenced by the inorganic nitrogen source (NH_4^+ and NO_3^-) with marked differences between mature and juvenile mycelium. In general, the biogeochemical transformation of copper bioaccumulated within the colony resulted in a more thermodynamically stable state and coordination environment of the potentially toxic metal.

Experimental procedures

Organism and media

Aspergillus niger van Tieghem (ATCC 201373), from the collection of the Geomicrobiology Group, School of Life Sciences, University of Dundee, was maintained on malt extract agar (MEA) at 25°C. Conidia were inoculated onto fresh MEA plates 24 h before experiments to ensure single colonies on the experimental plates. Then 7 mm diameter discs of mycelium aseptically cut, using a sterile cork borer, from the leading edge of the colonies were placed on top of cellophane membranes and grown on modified AP1 media with malachite in sterile Petri-dish microcosms at 25°C for up to 7 or 10 days. Prior to inoculation, 84 mm dia. discs of sterile cellophane membrane were placed aseptically on the surface of the agar in each Petri dish. AP1 media comprised KH_2PO_4 (3.67 mM), $MgSO_4 \cdot 7H_2O$ (0.811 mM), $CaCl_2 \cdot 6H_2O$ (0.228 mM), NaCl (1.711 mM), $FeCl_3 \cdot 6H_2O$ (0.925 μM), $ZnSO_4 \cdot 7H_2O$ (13.911 μM), $MnSO_4 \cdot 4H_2O$ (17.932 μM), $CuSO_4 \cdot 5H_2O$ (1.602 μM), D-glucose (20 g l^{-1}), agar no. 1 (Lab M, Bury, UK) (14 g l^{-1}) and a sole inorganic nitrogen source (37.8 mM) added either as ammonium ($(NH_4)_2SO_4$) or nitrate (KNO_3). To balance the increased levels of potassium in the NO_3 treatment 18.9 mM K_2SO_4 was added to the NH_4–containing medium. Prior to addition to the agar medium, to a final copper concentration equivalent to 10 mM, malachite [$Cu_2(CO_3)(OH)_2$] was pulverized to a grain size of less than 400 μm, ddH_2O-washed and sterilized with 70% (w/v) ethanol for 24 h followed by oven-sterilization at 80^{o}C for at least 24 h.

Evaluation of colony extension and mineral solubilization in agar

Growth, measured as extension of the colony radius and mineral solubilizing ability, measured as the radius of the clear solubilization zone in agar medium, were recorded every 2 days. The agar was also examined using light microscopy for observation of mineral solubilization and the formation of crystals.

Estimation of biomass yield, tolerance indices (TI) and copper bioaccumulation

Biomass of the colonies was measured every 2 days by peeling the biomass from the dialysis membrane, washing with cold ddH_2O, and oven-drying at 105°C until reaching constant weight. Metal tolerance was evaluated using a tolerance index (TI) as follows: (dry weight of malachite-exposed mycelium/dry weight of control mycelium × 100%) (Fomina *et al.*, 2005b). Samples of biomass (50 mg), powdered using a pestle and mortar (Milton Brook, Dorset, UK), were digested in 3.0 ml concentrated HNO_3 at 159 °C overnight at Grant BT5D heating block (Grant Instruments, Cambridge, UK). After appropriate dilution with ddH_2O, extracts were used for analysis of copper using atomic absorption spectroscopy (AAS) (Perkin Elmer AAnalyst 400 Atomic Absorption Spectrophotometer, Llantrisant, UK).

pH analysis

Once the biomass was removed, the surface pH profile of the agar was examined using an Orion 720A pH meter (Thermo Fisher Scientific, Loughborough, UK) fitted with a flat tip electrode (VWR International, Lutterworth, UK) taking measurements at 1 cm intervals across the entire diameter of the plate.

Examination of biominerals

Biomineralization of bioaccumulated copper in mycelium was examined using a Philips XL30 environmental scanning electron microscope (ESEM) (Philips BV, Amsterdam, Netherlands) field emission gun (FEG) operating at an accelerating voltage of 15 or 25 kV.

Sequential elution technique for copper evaluation in agar

The speciation of copper in agar was evaluated using a sequential elution technique (SET). Two agar squares (each 1x1 cm^2) were excised from the agar across the plate and subjected to a

stepwise procedure using 3 ml volumes of 5 different extractants: (i) water at 80°C (15 min); (ii) 2 M NaCl (30 min); (iii) 1 M NH_4OH (1 h), (iv) 1 M acetic acid (3 h) and (v) 1 M HCl (overnight). The samples were centrifuged (15 min, 4000 x g) (MSE Mistral 2000) between steps to collect the supernatant. Copper concentration in the samples was measured using AAS.

Determination of organic acids

Agar samples were used for determination of organic acid excretion. Two agar squares (each 1x1 cm^2) were digested in 6 ml of ddH_2O for 15 min at 80°C or in 6 ml of 1 M HCl overnight. After digestion 1 ml samples were removed, mixed with cation-exchange resin (Bio-Rad, AG 50W-X4, Bio-Rad Laboratories, Richmond, CA, USA) and filtered through a 0.45 μm pore size cellulose acetate membrane filter (Whatman, Maidstone, UK) into HPLC vials prior to analysis by HPLC (Waters 600E control with 717plus autosampler and 486 tunable wavelength detector, Watford, Herts, UK). Carboxylic acids were separated at room temperature using a BioRad Aminex® HPX-87H ion-exclusion column (300 mm x 7.8 mm) with a proton form guard column (Bio-Rad Laboratories, Richmond, CA, USA). The mobile phase used was 8 mM H_2SO_4 at a flow rate of 0.6 ml min^{-1}. Detection was carried out at 210 nm for 50 min. Acids were identified and quantified using the retention times and peak areas of a wide range of standards: acetic, *trans* and *cis*-aconitic, citric, formic, fumaric, galacturonic, gluconic, glucuronic, glutaconic, glycolic, glyoxylic, ketogluconic, lactic, maleic, malic, malonic, oxalic, propionic, pyruvic, salicylic, succinic and tartaric acid.

Microfocus XAS

To study the speciation of bioaccumulated copper, fragments of 5- and 10-day cultured *A. niger* colonies on ammonium- and nitrate-containing AP1 media were examined using XAS. XAS data were collected in microfocus mode operating at 2 Ge with an average current of 140 mA and a Si (111) monochromator at the CCLRC Daresbury Sychrotron Radiation Source (Daresbury, UK).

The beam was focused using two Kirkpatrick-Baez mirrors to a spot size of ~50 μm. Each sample was mounted on the beamline with the monochromator set at an energy of 12 keV. The sample was moved horizontally and vertically over a grid, collecting a full fluorescence spectrum at each point using a Canberra 13-element solid state detector. This produced a copper distribution map for each sample. The section was then positioned at chosen points in the map and fluorescence X-ray absorption spectra were collected at the copper K-edge. For most samples only XANES data were collected (to ca. 240 eV above the edge), but for a few selected areas with a higher copper concentration full EXAFS data were collected (to ca. 640 eV above the edge) as described previously (Fomina *et al*., 2007a). The data were background subtracted and normalised. EXAFS data were analysed using EXCURV98 using full curved wave theory (Gurman *et al*., 1984; Binsted, 1998). XANES data were compared with XANES data from selected model compounds in order to determine the most likely oxidation state and coordination environment of the copper.

Statistical analysis

All data presented in the paper are the means of at least three replicates and error bars represent one standard error either side of the mean. SigmaStat (Release 3.1) was used to perform statistical analyses.

Acknowledgements

The authors gratefully acknowledge funding from BBSRC/BIRE programme (94/BRE13640), the BBSRC postgraduate research studentship (ADB) and CCLRC Daresbury SRS user grants. We thank Dr Andrew Bennett (CCLRC Daresbury SRS) for invaluable help with collecting and analysing microfocus XAS data. G. M. Gadd also gratefully acknowledges an award under the Chinese Government's 1000 Talents Plan with the Xinjiang Institute of Ecology and Geography, Chinese Academy of Sciences, Urumqi, China.

References

Arnott, H.J. (1995) Calcium oxalate in fungi. In *Calcium Oxalate in Biological Systems*, Khan, S.R. (ed). Boca Raton, FL, USA: CRC Press, pp. 73-111.

Bellion, M., Courbot, M., Jacob, C., Blaudez, D., and Chalot, M. (2006) Extracellular and cellular mechanisms sustaining metal tolerance in ectomycorrhizal fungi. *FEMS Microbiol Lett* **254:** 173–181.

Binsted, N. (1998) Daresbury Laboratory EXCURV98 Program.

Bordas, J., Koch, M.H.J., Hartmann, H.J., and Wester, U. (1983) Tetrahedral copper-sulfur co-ordination in yeast copper-thionein, an EXAFS study. *FEBS Lett* **140:** 19-21.

Bücking, H., and Heyser, W. (1999) Elemental composition and function of polyphosphates in ectomycorrhizal fungi – an X-ray microanalytical study. *Mycol Res* **103:** 31–39.

Carrodus, B.B. (1967) Absorption of nitrogen by mycorrhizal roots of beech. II. Ammonium and nitrate as sources of nitrogen. *New Phytol* **66:** 1-4.

Dumestre, A., Sauve´, S., McBride, M., Baveye, P., and Berthelin, J. (1999) Copper speciation and microbial activity in long-term contaminated soils. *Arch Environ Contam Toxicol* **36:** 124–131.

Fomina, M.A., Alexander, I.J., Hillier, S., and Gadd, G.M. (2004) Zinc phosphate and pyromorphite solubilization by soil plant-symbiotic fungi. *Geomicrobiol J* **21:** 351–366.

Fomina, M., Hillier, S., Charnock, J.M., Melville, K., Alexander, I.J., and Gadd, G.M. (2005a) Role of oxalic acid overexcretion in toxic metal mineral transformations by *Beauveria caledonica*. *Appl Environ Microbiol* **71:** 371–381.

Fomina, M.A., Alexander, I.J., Colpaert, J.V., and Gadd, G.M. (2005b) Solubilization of toxic metal minerals and metal tolerance of mycorrhizal fungi. *Soil Biol Biochem* **37:** 851–866.

Fomina, M., Charnock, J., Bowen, A.D., and Gadd, G.M. (2007a) X-ray absorption spectroscopy (XAS) of toxic metal mineral transformations by fungi. *Environ Microbiol* **9:** 308–321.

Fomina M., and Gadd, G.M. (2007b) Metal and mineral transformations: a mycoremediation perspective. In *Exploitation of Fungi*, Robson, G.D., Van West, P. and Gadd, G.M. (eds). Cambridge, UK: Cambridge University Press, pp. 236-254.

Gadd, G.M. (1993) Interactions of fungi with toxic metals. *New Phytol* **124:** 25–60.

Gadd, G.M. (1999) Fungal production of citric and oxalic acid: importance in metal speciation, physiology and biogeochemical processes. *Adv Microb Physiol* **41:** 47-92.

Gadd, G.M. (2007) Geomycology: biogeochemical transfomations of rocks, minerals, metals and radionuclides by fungi, bioweathering and bioremediation. *Mycol Res* **111:** 3–49.

Gadd, G.M., Bahri-Esfahania, J., Li, Q., Rhee, Y.J., Wei, Z., Fomina, M., and Liang, X. (2014) Oxalate production by fungi: significance in geomycology, biodeterioration and bioremediation. *Fungal Biol Rev* **28:** 36-55.

Goetghebeur, M., Kermasha, S., Kensley, J., and Metche, M. (1995) Purification and characterization of copper-metallothionein from *Aspergillus niger* by affinity chromatography. *Biotechnol Appl Biochem* **22:** 315-325.

Gurman, S.J., Binsted, N., and Ross, I. (1984) A rapid, exact, curved-wave theory for EXAFS calculations. *J Phys Chem C* **17:** 143–151.

van Hees, P.A.W., van Hees, A.M.T., and Lundström U.S. (2001) Determination of aluminium complexes of low molecular weight organic acids in soil solution from forest soils using ultrafiltration. *Soil Biol Biochem* **33:** 867-874.

Jones, D.L. (1998) Organic acids in the rhizosphere - a critical review. *Plant Soil* **205:** 25-44.

Kermasha, S., Pellerin, F., Rovel, B., Goetghebeur, M., and Metche, M. (1993) Purification and characterization of copper-metallothioneins from *Aspergillus niger*. *Biosci Biotechnol Biochem* **57:** 1420-1423.

Kornberg, A., Rao, N.N., and Ault-Riché, D. (1999) Inorganic polyphosphate: a molecule of many functions. *Annu Rev Biochem* **68:** 89-125.

Kritzman, G., Chet, I. and Henis, Y. (1977) The role of oxalic acid in the pathogenic behaviour of *Sclerotium rolfsii* Sacc. *Exp Mycol* **1:** 280-285.

Lapeyrie, F., Chilvers, G.A., and Bhem, C.A. (1987) Oxalic acid synthesis by the mycorrhizal fungus *Paxillus involutus* (Batsch, ex Fr.) Fr. *New Phytol* **106:** 139-146.

Orlovich, D.A. and Ashford, A.E. (1993) Polyphosphate granules are an artefact of specimen preparation in the ectomycorrhizal fungus *Pisolithus tinctorius*. *Protoplasma* **173:** 91-102.

Outten, F.W., Huffman, D.L., Hale, J.A., and O'Halloran, T.V. (2001) The independent cue and cus systems confer copper tolerance during aerobic and anaerobic growth in *Escherichia coli*. *J Biol Chem* **276:** 30670-30677.

Rensing, C., and Grass, G. (2003) *Escherichia coli* mechanisms of copper homeostasis in a changing environment. *FEMS Microbiol Rev* **27:** 197-213.

Roelofs, R.F.R., Rengel, Z., Cawthray, G.R., Dixon, K.W., and Lambers, H. (2001) Exudation of carboxylates in Australian Proteaceae: chemical composition. *Plant Cell Environ* **24:** 891-904.

Saito, K., Ohtomo, R., Kuga-Uetake, Y., Aono, T., and Saito, M. (2005) Direct labeling of polyphosphate at the ultrastructural level in *Saccharomyces cerevisiae* by using the affinity of the polyphosphate binding domain of *Escherichia coli* exopolyphosphatase. *Appl Environ Microbiol* **71:** 5692-5701.

Saito, K., Kuga-Uetake, Y., Saito, M., and Peterson, R.L. (2006) Vacuolar localization of phosphorus in hyphae of *Phialocephala fortinii*, a dark septate fungal root endophyte. *Can J Microbiol* **52:** 643-650.

Tsekova, K., Galabova, D., Todorova, K., and Ilieva, S. (2002) Phosphatase activity and copper uptake during the growth of *Aspergillus niger*. *Process Biochem* **37:** 753–758.

Tsekova, K., and Galabova, D. (2003) Phosphatase production and activity in copper (II) accumulating *Rhizopus delemar*. *Enzyme Microb Technol* **33:** 926–931.

Wang, X., Chen, Q., Hu, H., Yin, Z., and Xiao, Z. (2009) Solubility prediction of malachite in aqueous ammoniacal ammonium chloride solutions at 25°C. *Hydrometallurgy* **99:** 231–237.

Table 1. Distribution of copper between fungal biomass and different fractions of copper in the agar medium after growth of *A. niger* for 7 days on malachite-amended medium with different inorganic sources of nitrogen. Values present the averages calculated using the data shown on Figs.1C,D; 2 and 4A (n=3, ±SEM does not exceed 15%).

Copper fraction	Proportion of copper (%)	
	Ammonium medium	Nitrate medium
H_2O	48.5	28.1
NaCl	4.6	22.8
NH_4OH-malachite	0.3	19.8
NH_4OH-oxalate	8.2	16.5
CH_3COOH	1.1	4.3
Cu accumulated by biomass	37.3	8.4

Legends to Figures

Fig. 1. Growth, mineral solubilization, copper accumulation and medium acidification during *A. niger* growth with 10 mM malachite and different inorganic sources of nitrogen. (A,B) colony extension in the absence (grey triangles) or presence (black squares) of malachite; solubilization halo (grey circles) on (A) ammonium and (B) nitrate; (C) biomass yield and (D) copper bioaccumulation on ammonium (black diamonds) and nitrate (grey squares); and (E, F) pH changes in the agar medium with (E) ammonium and (F) nitrate showing data for the abiotic control (light grey circles), day 1 (black circles), day 3 (dark grey squares), day 5 (grey diamonds) and day 7 (grey triangles). The bars indicate the standard error of the mean (SEM) (n=3); where error bars are not shown, they were less than the dimensions of the symbols.

Fig. 2. Changes in the amounts of copper in different fractions eluted from the agar medium during growth of *A. niger* with 10 mM malachite and different inorganic sources of nitrogen. (A) ammonium and (B) nitrate: water fraction (white circles), NaCl-fraction (dark grey squares), NH_4OH-fraction (black triangles), acetic acid fraction (dark grey diagonal crosses), HCl-fraction (grey asterisks), and HNO_3-fraction (light grey circles). The error bars indicate the SEM (n=3); where error bars are not shown, they were less than the dimensions of the symbols.

Fig. 3. Spatial distribution of (A) the NH_4OH-fraction of copper representing mineral phase(s) in the agar and (B) the H_2O-fraction of copper representing soluble phase(s) during *A. niger* growth with malachite and different inorganic sources of nitrogen: ammonium and nitrate. Representative results are shown from one of at least three determinations.

Fig.4. Distribution of oxalate in the agar medium as a function of nitrogen source, time and distance from fungal colony centre in agar medium during *A. niger* growth with malachite and

different inorganic sources of nitrogen. (A) water- and HCl-extractable oxalate, (B) total oxalate and (C) the proportion as water-extractable oxalate in agar medium during *A. niger* growth with malachite and different inorganic sources of nitrogen. The symbols in panel (A) denote data for oxalate in water (white symbols) and HCl (black symbols), in agar media containing fractions for ammonium (circles), and or nitrate (triangles) as a N source; (B) and (C) denote data for agar media with ammonium (black squares) and or nitrate (white diamonds). Where visible, the error bars indicate one SEM (n=3); where error bars are not shown, they were less than the dimensions of the symbols.

Fig. 5. Microfocus XAS/XANES analysis of chemical speciation of copper bioaccumulated by a 5 day old colony of *A. niger* grown with malachite on ammonium-containing medium. Analysis was performed at points selected in the central zone and periphery of the colony. (A) Colony morphology with designation of the fragment excised for analysis (red frame) ; (B) XAS copper mapping of the excised fragment showing the sites chosen for analysis in the colony centre (blue and purple circles) and in the periphery (green, yellow and red circles) visualizing copper distribution. The highest copper concentration shows as white and a decrease in copper shows as gradually darkening tones of green; (C) XAS spectra for the chosen sites and (D) detailed XANES spectra of the absorption edge. Typical data are shown from one of at least three determinations.

Fig. 6. Spatio-temporal changes in speciation of copper bioaccumulated within the central (dark grey) and the peripheral (light grey) zones of the *A. niger* colonies exposed to malachite depending on the inorganic source of nitrogen in the medium. Typical data are shown from one of at least three determinations.

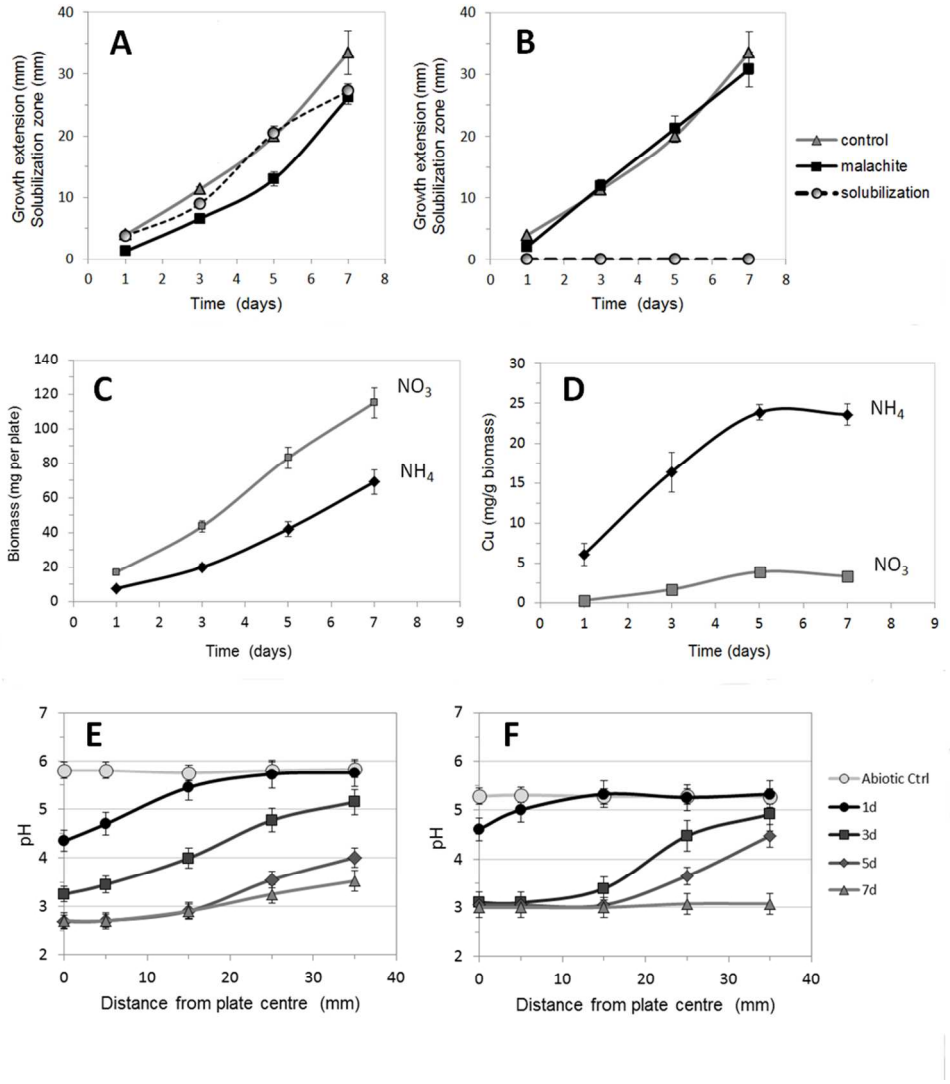

Fig. 1. Growth, mineral solubilization, copper accumulation and medium acidification during A. niger growth with 10 mM malachite and different inorganic sources of nitrogen. (A,B) colony extension in the absence (grey triangles) or presence (black squares) of malachite; solubilization halo (grey circles) on (A) ammonium and (B) nitrate; (C) biomass yield and (D) copper bioaccumulation on ammonium (black diamonds) and nitrate (grey squares); and (E, F) pH changes in the agar medium with (E) ammonium and (F) nitrate showing data for the abiotic control (light grey circles), day 1 (black circles), day 3 (dark grey squares), day 5 (grey diamonds) and day 7 (grey triangles). The bars indicate the standard error of the mean (SEM) (n=3); where error bars are not shown, they were less than the dimensions of the symbols.

400x450mm (72 x 72 DPI)

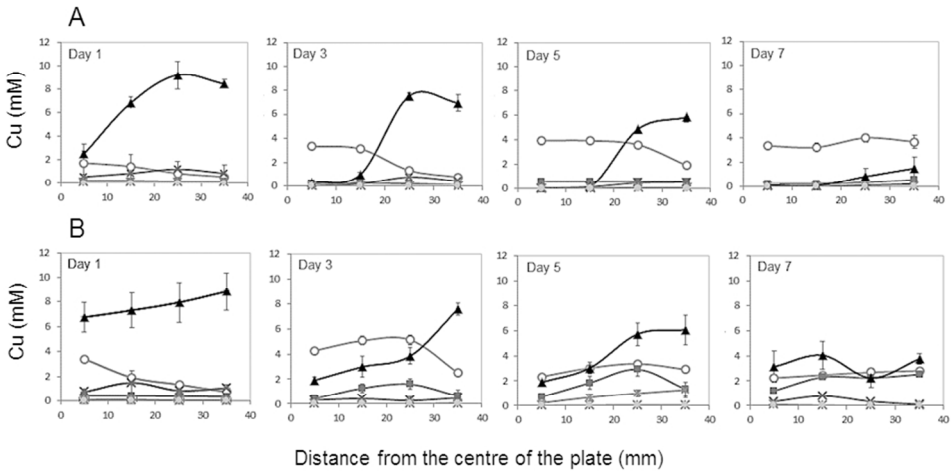

Fig. 2. Changes in the amounts of copper in different fractions eluted from the agar medium during growth of A. niger with 10 mM malachite and different inorganic sources of nitrogen. (A) ammonium and (B) nitrate: water fraction (white circles), NaCl-fraction (dark grey squares), NH4OH-fraction (black triangles), acetic acid fraction (dark grey diagonal crosses), HCl-fraction (grey asterisks), and HNO3-fraction (light grey circles). The error bars indicate the SEM (n=3); where error bars are not shown, they were less than the dimensions of the symbols.

353x189mm (72 x 72 DPI)

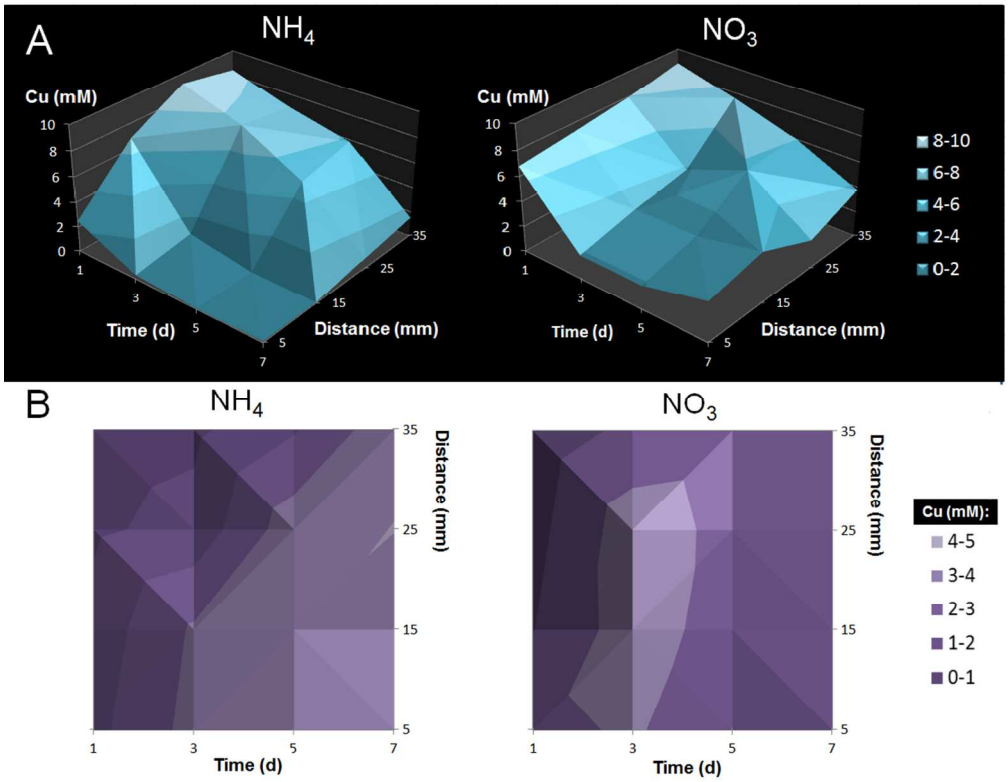

Fig. 3. Spatial distribution of (A) the NH4OH-fraction of copper representing mineral phase(s) in the agar and (B) the H2O-fraction of copper representing soluble phase(s) during A. niger growth with malachite and different inorganic sources of nitrogen: ammonium and nitrate. Representative results are shown from one of at least three determinations.

412x339mm (72 x 72 DPI)

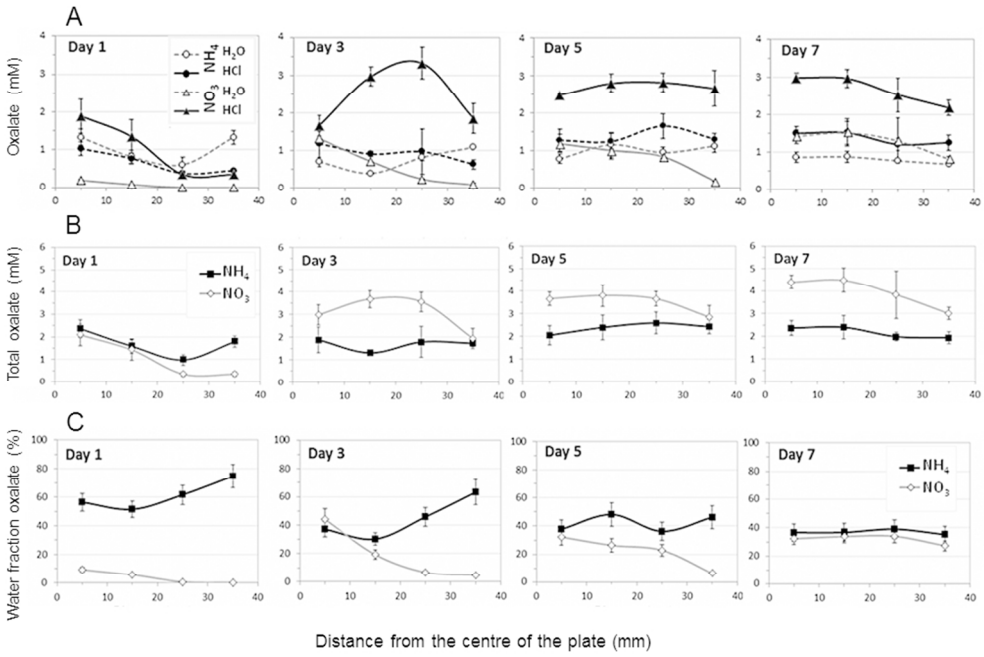

Fig.4. Distribution of oxalate in the agar medium as a function of nitrogen source, time and distance from fungal colony centre in agar medium during A. niger growth with malachite and different inorganic sources of nitrogen. (A) water- and HCl-extractable oxalate, (B) total oxalate and (C) the proportion as water-extractable oxalate in agar medium during A. niger growth with malachite and different inorganic sources of nitrogen. The symbols in panel (A) denote data for oxalate in water (white symbols) and HCl (black symbols), in agar media containing fractions for ammonium (circles), and or nitrate (triangles) as a N source; (B) and (C) denote data for agar media with ammonium (black squares) and or nitrate (white diamonds). Where visible, the error bars indicate one SEM (n=3); where error bars are not shown, they were less than the dimensions of the symbols.

360x242mm (72 x 72 DPI)

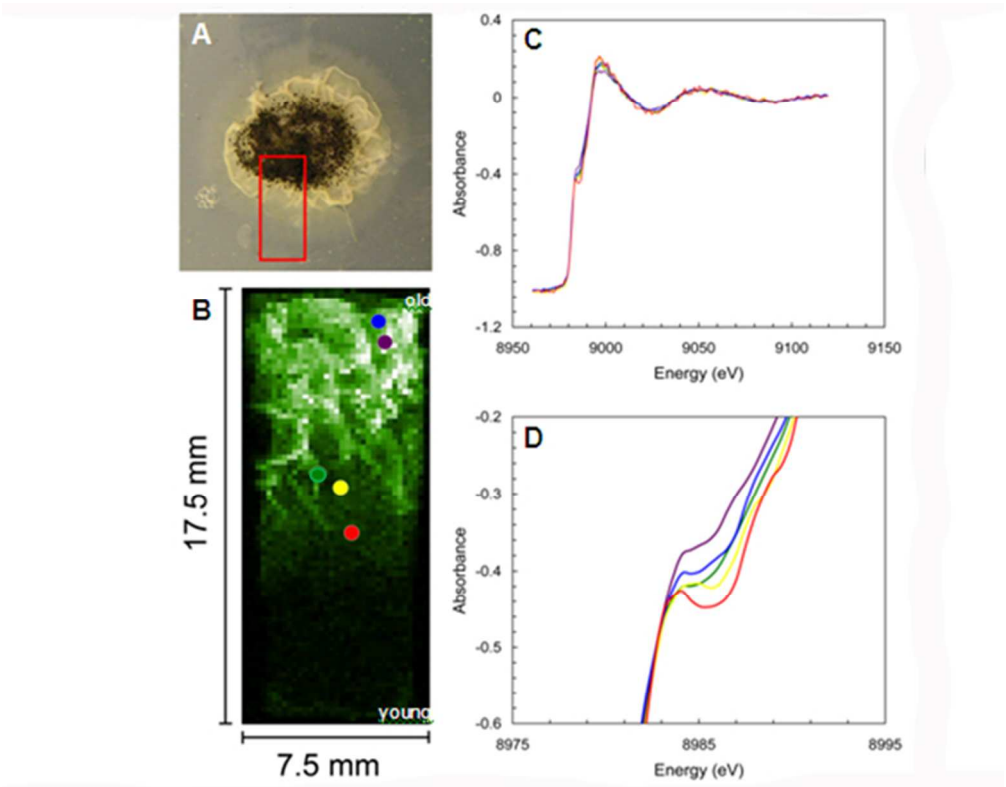

Fig. 5. Microfocus XAS/XANES analysis of chemical speciation of copper bioaccumulated by a 5 day old colony of A. niger grown with malachite on ammonium-containing medium. Analysis was performed at points selected in the central zone and periphery of the colony. (A) Colony morphology with designation of the fragment excised for analysis (red frame) ; (B) XAS copper mapping of the excised fragment showing the sites chosen for analysis in the colony centre (blue and purple circles) and in the periphery (green, yellow and red circles) visualizing copper distribution. The highest copper concentration shows as white and a decrease in copper shows as gradually darkening tones of green; (C) XAS spectra for the chosen sites and (D) detailed XANES spectra of the absorption edge. Typical data are shown from one of at least three determinations.

186x147mm (95 x 95 DPI)

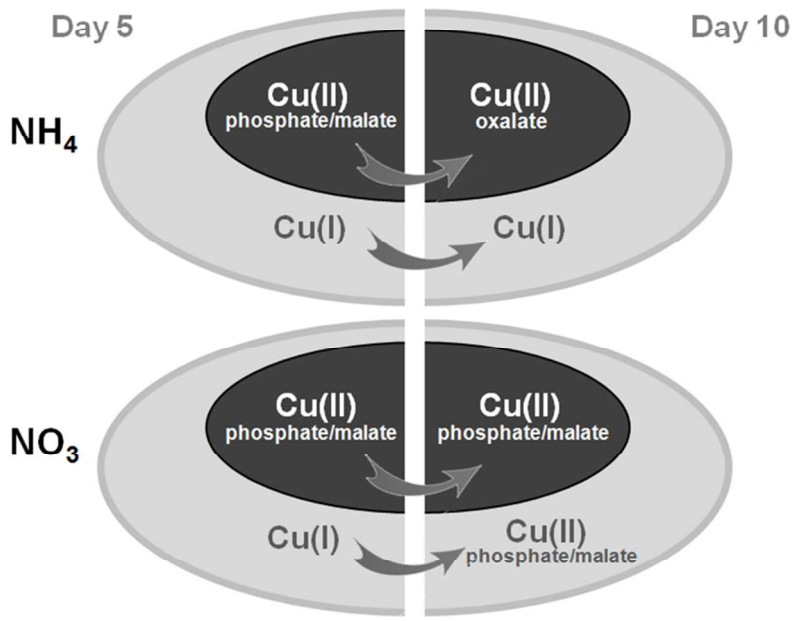

Fig. 6. Spatio-temporal changes in speciation of copper bioaccumulated within the central (dark grey) and the peripheral (light grey) zones of the A. niger colonies exposed to malachite depending on the inorganic source of nitrogen in the medium. Typical data are shown from one of at least three determinations.

351x260mm (72 x 72 DPI)